RESEARCH PAPER

L-Carnosine-coated nanoceria promotes proliferation of human embryonic lung fibroblasts via STAT3/BCL2 axis activation

Elena V. Proskurnina[1,2*], Madina M. Sozarukova[1], Elizaveta S. Ershova[3], Natalia N. Veiko[3], Matvei A. Popkov[1], Edmund V. Kostyuk[1], Vladimir K. Ivanov[1], Svetlana V. Kostyuk[1,3]

[1]Kurnakov Institute of General and Inorganic Chemistry of the Russian Academy of Sciences, Moscow, Russia
[2] Faculty of Chemistry, Biology and Biotechnology, North Ossetian State University named after Kosta Levanovich Khetagurov, Vladikavkaz, Russia
[3] Institute of Longevity with a Clinic of Rehabilitation and Preventive Medicine, Russian Scientific Center of Surgery named after Academician B.V. Petrovsky, Moscow, Russia

ABSTRACT

Background: Nanoceria exhibits unique catalytic activity toward reactive oxygen species (ROS), mimicking the functions of natural enzymes—a property that underlies its biomedical applications, given the essential role of ROS in living organisms. Carnosine is a pH buffer with intrinsic antioxidant properties; it chelates metals and binds carbonyl compounds.
Objective(s): Using human embryonic lung fibroblast model, this study investigates the impacts of carnosine-conjugated nanoscale CeO_2 on cell survival, cellular oxidative status, ROS-induced DNA oxidation, dual-strand DNA breaks, activation of DNA repair response, and gene and protein expression of NOX4, NRF2, STAT3, as well as proliferation and autophagy markers.
Results: Carnosine-conjugated nanoceria proved to be non-cytotoxic at millimolar concentrations. Its effects on cytotoxicity, genotoxicity, DNA repair, mitochondrial membrane potential, autophagy, and NOX4 and NRF2 expression were similar to those of bare nanoceria. The principal differences were observed in the expression of STAT3, PCNA, and BCL2 proteins, where carnosine-coated nanoceria induced a pronounced activating impact after 24 h of exposure, thus promoting proliferation and increasing concentration of the PCNA proliferation marker.
Conclusion: We hypothesize that carnosine-coated nanoceria directly activates the STAT3/BCL2 axis. These findings may facilitate the development of new molecular models for studying signaling pathways and advance in characterization of the nanoceria's biochemical roles in regulating ROS-driven cellular pathways. Moreover, carnosine-coated nanoceria could be considered a potential agent for enhancing the survival of cell cultures—such as hematopoietic cultures intended for transplantation—through activation of the STAT3/BCL2 axis.

Keywords*: Ceric oxide; carnosine; cell proliferation; reactive oxygen species; fibroblasts*

How to cite this article
Proskurnina E.V, Sozarukova M.M, Ershova E.S, Veiko N.N, Popkov M.A, Kostyuk E.V, Ivanov V.K, Kostyuk S.V. L-Carnosine-coated nanoceria promotes proliferation of human embryonic lung fibroblasts via STAT3/BCL2 axis activation. Nanomed J. 2026; 13: 1-. DOI: 10.22038/NMJ.2026.90673.2292

ABBREVIATIONS

BRCA1: breast cancer type 1 susceptibility protein; ***DCF:*** 2′,7′-dichlorofluorescein; ***DLS:*** dynamic light scattering; ***FTIR-ATR:*** Fourier transform infrared spectroscopy with attenuated total reflectance; **γH2AX:** H2A histone family member X; ***H2DCFH-DA:*** 2′,7′-dichlorodihydrofluorescein diacetate; ***IL:*** interleukin; ***JAK:*** Janus kinase; ***LC3:*** 1A/1B-light chain 3; ***MAPK:*** mitogen-activated protein kinase; ***MTT:*** 3-(4,5-Dimethylthiazol-2-yl)-2,5-diphenyltetrazolium bromide; ***NF-κB:*** nuclear factor kappa-light-chain-enhancer of activated B cells; ***NOX4:*** NADPH oxidase 4; ***NRF2:*** nuclear factor erythroid 2-related factor 2; ***8-oxo-dG:*** 8-oxo-2′-deoxyguanosine; ***PBS:*** phosphate-buffered saline; ***PCNA:*** proliferating cell nuclear antigen; qRT-PCR, real-time quantitative reverse transcription polymerase chain reaction; ***ROS:*** reactive oxygen species; ***SOCS3:*** suppressor of cytokine signaling 3; ***STAT3:*** signal transducer and activator of transcription 3; ***TMRM:*** tetramethylrhodamine, methyl ester; ***XRD:*** X-ray diffraction; ***VEGF:*** vascular endothelial growth factor

INTRODUCTION

Cerium dioxide nanoparticles (nanoceria) exhibit unique catalytic activity toward reactive oxygen species (ROS), mimicking natural enzymes—a property that underlies all biomedical applications of nanoceria, given the crucial role of ROS in living systems (1) (2). Depending on the

* *Corresponding author:* Elena V. Proskurnina, Professor, Kurnakov Institute of General and Inorganic Chemistry of the Russian Academy of Sciences, Moscow, Russia. E-Mail address: proskurnina@gmail.com.
Note. This manuscript was submitted on August 22, 2025; approved on November 25, 2025.

surface coating and environmental conditions, nanoceria may exert either anti- or pro-oxidant effects. In cancer cells under low-pH conditions, nanoceria functions as an ROS generator, cytotoxic agent, and even radiosensitizer (3) (4). Additionally, nanoceria generates molecular oxygen within tumors, sensitizing malignant cells to light- and radio-based therapy, as well as to chemotherapeutic interventions (5). In normal cells, nanoceria has anti-inflammatory and antibacterial activity, supporting its use in tissue engineering (6). Both bare and functionalized nanoceria demonstrate strong potential to accelerate healing in acute and chronic wounds (7). Furthermore, nanoceria has been proposed as an antidiabetic agent (3) and a protective drug in retinal macular degeneration (8).

The application of nanoceria carries toxicological risks that depend on the route of exposure, dose, and chemical composition of the nanoparticles. Being a non-degradable compound, nanoceria persists in organs for a long time (at least for several months) with slow elimination rates. The acute toxicity of nanoceria is quite low, but accumulated nanoparticles can cause granuloma and fibrosis in the lungs and granuloma in the liver (9). Owing to its biostability, there is a risk of adverse effects from prolonged exposure to this nanomaterial; consequently, surface modification of ceria nanoparticles is generally required for biomedical applications.

Carnosine is an essential endogenous dipeptide predominantly found in skeletal muscle, the central nervous system, olfactory neurons, and the lens of the eye in various vertebrates, including humans (10). It functions as a pH buffer and possesses intrinsic antioxidant properties; it chelates metals such as iron and copper and binds to carbonyl compounds, which are advanced glycation and lipoperoxidation end products (11) (12) (13). Carnosine has been shown to improve muscle function in athletes (14), myocardial function (15), and vascular health (16). Additionally, it plays active roles in bone physiology and biochemistry (17), acts as a neuroprotector (18), and inhibits oxidative stress (19). Carnosine activates the NRF2 anti-inflammatory pathway (20) (21), which contributing to its beneficial effects (22) (23). Moreover, carnosine exhibits anti-aging properties (24), slowing the aging process of cultured human diploid fibroblasts by modulating protein metabolism (25) (26). Cells cultured in the presence of carnosine display a slower rate of telomere shortening and an extended lifespan (27).

Carnosine is also utilized to functionalize various nanomaterials. For example, carnosine functionalization significantly increases the solubility of carbon nanotubes, enhancing their biomedical applications (28). It enhances the antibacterial activity of graphene oxide (29). Magnetic nanoparticles coated with L-carnosine have been developed to amplify the chemotherapeutic efficacy of the dipeptide (30). Furthermore, Fe_3O_4 magnetic nanoparticles functionalized with L-carnosine and loaded with dexamethasone have emerged as an effective drug delivery platform in ischemic stroke (31). Hydrolyzed polyacrylonitrile nanofibers functionalized with L-carnosine and loaded with zinc oxide nanoparticles have been employed in the development of an anti-melanoma wound dressing (32).

Therefore, carnosine-coated nanoceria represents a promising hybrid compound that combines the advantageous biochemical properties of both carnosine and nanoceria. Understanding how surface modifications influence the performance and biocompatibility of nanoscale CeO_2 is essential to evaluate its advantages and risks associated with its biomedical applicability. However, studies on the impacts of carnosine-coated nanoceria on human gene expression are scarce or nonexistent. Human embryonic lung fibroblasts represent a robust and sensitive in vitro system for investigating the genetic effects of nanosubstances. Using human embryonic lung fibroblasts, this study investigates the impacts of carnosine-conjugated nano-CeO_2 on cell survival, cellular oxidative status, ROS-induced DNA oxidation, dual-strand DNA breaks, activation of DNA repair response, and gene and protein expression of NADPH-oxidase 4 (NOX4), nuclear factor erythroid 2-related factor 2 (NRF2), signal transducer and activator of transcription 3 (STAT3), as well as proliferation and autophagy markers.

MATERIALS AND METHODS

Preparation of pristine and carnosine-conjugated CeO_2 nanoparticles

An aqueous cerium dioxide (CeO_2) sol was prepared by thermal hydrolysis of $(NH_4)_2[Ce(NO_3)_6]$ (#215473, Sigma, St. Louis, MO, USA) (33). Briefly, a 100 g/L salt solution was incubated at 95 °C for 24 hours, resulting in the precipitation of cerium dioxide. The precipitate was subjected to three consecutive washes with isopropanol and redispersed in distilled water. Remaining isopropanol was boiled off at 100°C under constant stirring for 1 h.

A solution of L-carnosine (β-alanyl-L-histidine, #305-84-0, Sigma, St. Louis, MO, USA) was prepared by dissolving carnosine in distilled water.

Carnosine-conjugated nano-CeO_2 was synthesized by gradual addition the CeO_2 sol to the ligand solution under constant stirring. The molar ratio of components in the final CeO_2 sol was 1:1. The pH adjustment of the suspension to 7.4 was performed using aqueous NH_3.

Materials characterization

Concentration Determination

Quantification of the CeO_2 sol concentration was performed gravimetrically. Portions were transferred into pre-weighed crucibles, evaporated in a box furnace, and subsequently heated at 900 °C for 240 min until constant weight.

X-Ray Powder Diffraction (XRD)

Using a Bruker D8 Advance diffractometer (CuKα line), XRD characterization of the dried CeO_2 samples was performed across a 2θ angular range of 3 to 120°, at step sizes between 0.01° and 0.02°, with data acquisition lasting at least 0.3 seconds for each step.

Particle Size Distribution and ζ-Potential

Particle size range characterization and ζ-potential were measured on a Photocor Compact-Z analyzer (Photocor, Moscow, Russia) using a 636.65 nm laser at 20 °C. For each sample, the autocorrelation function was obtained by averaging 10 individual runs (20 s each). The hydrodynamic radius was calculated using the regularization algorithm implemented in DynalS software.

UV–Visible Spectroscopy

Using 10-mm quartz cuvettes, UV–Vis absorption was measured from 200 to 800 nm at 1 nm intervals on an SF-2000 spectrophotometer (OKB SPECTR LLC, St. Petersburg, Russia) employing a deuterium–halogen lamp.

Fourier Transform Infrared Spectroscopy (FTIR)

Binding of ligand molecules to the nanoparticle surface was assessed using FTIR spectroscopy. Spectra were acquired in the 400–4000 cm^{-1} range at 2 cm^{-1} resolution with an InfraLUM FT-08 spectrometer (Lyume'ks, St. Petersburg, Russia).

Cultivation of cells

The 4th-passage human embryonic lung fibroblasts were obtained from the Research Centre for Medical Genetics (Moscow, Russia) and maintained in Dulbecco's Modified Eagle's Medium (DMEM; PanEco, Moscow, Russia) containing 10% fetal bovine serum (PAA, Vienna, Austria), 50 U/mL penicillin, 50 μg/mL streptomycin, and 10 μg/mL gentamicin. Cells were suspended at a concentration of 17,000 cells/mL. The cells were maintained in culture at 37 °C for 24 hours before nanoparticle exposure. Uncoated nanoceria or carnosine-conjugated nanoceria were then added, next cells were incubated for 1, 3, 24, or 72 h. Negative controls used cell cultures without nanoparticles. Positive controls included 10% dimethyl sulfoxide (Sigma, St. Louis, MO, USA) for the MTT assay and interleukin-6 (10 ng/mL, Sigma, St. Louis, MO, USA) to evaluate the induction of the STAT3 signaling cascade.

Viability of cells and evaluation of mitochondrial membrane potential

Cell viability determination was performed via a 72-hour MTT assay with 3'-(4,5-dimethylthiazol-2-yl)-2,5-diphenyl tetrazolium bromide. Absorbance at 550 nm was measured using an EnSpire plate reader (PerkinElmer, Turku, Finland). Control cells were maintained nanoparticle-free.

Mitochondrial membrane potential was evaluated using tetramethylrhodamine methyl ester (TMRM; Thermo Fisher Scientific, Waltham, MA, USA) according to previously described protocols (34).

Fluorescence microscopy

Fluorescence micrographs were captured using an Axio Imager A2 microscope (Carl Zeiss, Oberkochen, Germany). Approximately 5×10^5 cells were plated in slide-bottom flasks. Cells were washed with PBS (phosphate-buffered saline) following medium removal, then incubated with 2',7'-dichlorodihydrofluorescein diacetate (H_2DCFDA; stock concentration 2 mg/mL in PBS, diluted 1:200) for 15 min, and washed again with PBS. No fewer than 100 fields, selected at random, were examined. Signal collection lasted from 6 to 10 seconds. Images were processed using the ZEN 3.10 software platform (Carl Zeiss, Oberkochen, Germany).

Flow cytometric measurement

Cellular reactive oxygen species

Cellular reactive oxygen species were quantified with flow cytometry. Cells were incubated with 10 μM H_2DCFH-DA in PBS (Molecular Probes/Invitrogen, Carlsbad, CA, USA) for 15 minutes in darkness, followed by PBS washing, resuspension in PBS, and flow cytometric analysis in the FITC channel on a CytoFLEX S flow cytometer (Beckman Coulter, Brea, CA, USA).

Expression of proteins and markers

Following washing with Versene solution (Thermo Fisher Scientific, Waltham, MA, USA), cells

were incubated with 0.25% trypsin (PanEco, Moscow, Russia), washed with culture medium, resuspended in PBS with pH 7.4 (PanEco, Moscow, Russia), and fixed using paraformaldehyde (Sigma-Aldrich, St. Louis, MO, USA) at 37°C for 10 min. Cells were subjected to three washes with 0.5% BSA-PBS, permeabilized either by 0.1% Triton X-100 in PBS for 15 minutes at room temperature (20 °C) or by 90% methanol at 4 °C, and subsequently washed three additional times with 0.5% BSA-PBS. The cell samples were treated with 1 μg/mL conjugated primary antibodies for 2 hours at room temperature, followed by PBS washing and flow cytometric analysis.

Primary antibodies were as follows: DyLight488-γH2AX (pSer139) (nb100-78356G, NovusBio, Centennial, CO, USA), FITC-NRF2, (bs1074r-fitc, Bioss Antibodies Inc. Woburn, MA, USA), FITC-BRCA1 (Nb100-598F, NovusBio, Centennial, CO, USA), PE-8-oxo-dG (sc-393871 PE, Santa Cruz Biotechnology, Dallas, TX, USA), CY5.5-NOX4 (bs-1091r-cy5-5, Bioss Antibodies Inc. Woburn, MA, USA), A350-BCL2 (bs-15533r-a350, Bioss Antibodies Inc. Woburn, MA, USA), LC3 (NB100-2220 NovusBio, Centennial, CO, USA), and PCNA (ab2426, Abcam plc, Cambridge, UK).

Secondary antibody: anti-rabbit IgG-FITC (sc-2359, Santa Cruz Biotechnology, Dallas, TX, USA).

Quantitative mRNA analysis

Total RNA was isolated using the RNeasy Mini Kit (Qiagen, Hilden, Germany), treated with DNase I, and reverse-transcribed using the Reverse Transcriptase Kit (Sileks, Moscow, Russia). Quantitative reverse transcription PCR (qRT-PCR) with SYBR Green PCR Master Mix (Applied Biosystems, Foster City, CA, USA) was performed on a StepOnePlus system (Applied Biosystems), using *TBP* as the reference gene.

Primers were as follows (Sintol, Moscow, Russia): *BAX* (F: CCCGAGAGGTCTTTTTCCGAG, R: CCAGCCCATGATGGTTCTGAT); *BCL2* (F: TTTGGAAATCCGACCACTAA; R: AAAGAAATGCAAGTGAATGA); *NRF2* (NFE2L2) (F: TCCAGTCAGAAACCAGTGGAT, R: GAATGTCTGCGCCAAA AGCTG); *NOX4* (F: TTGGGGCTAGGATTGTGTCTA; R: GAGTGTTCGGCACATGGGTA); *STAT3* (F: GGGTGGAGAAGGACATCAGCGGTAA, R: GCCGACAATACTTTCCGAATGC); *Ki-67* (F: ACGCCTGGTTACTATCAAAAGG; R: CAGACCCATTTACTTGTGTTGGA); *NF-κB1* (F: CAGATGGCCCATACCTTCAAAT; R: CGGAAACGAAATCCTCTCTGTT); *BRCA1* (F: TGTGAGGCACCTGTGGTGA, R: CAGCTCCTGGCACTGGTAGAG); and *TBP* (reference gene) (F: GCCCGAAACGCCGAATAT, R: CCGTGGTTCGTGGCTCTCT).

Statistics

Results represent the mean ± standard deviation of three separate experiments. The non-parametric Mann–Whitney U test with Bonferroni correction was applied to assess statistical significance. Taking the Bonferroni correction into account, a *p*-value below 0.004 indicated statistical significance. The calculations were performed with StatPlus 2007 Pro v4.9.2 software (AnalystSoft Inc., Walnut, CA, USA).

RESULTS

Synthesis and physicochemical characterization of nanoparticles

Bare cerium dioxide samples were prepared via thermal hydrolysis of a solution containing $(NH_4)_2[Ce(NO_3)_6]$ (33). The resulting cerium dioxide sol had a concentration of 0.130 ± 0.004 mol/L (22 g/L).

Figure S1a (see Supplementary Information, Figure S1a) presents the X-ray diffraction (XRD) patterns for cerium dioxide sols dried at 50°C and for pure carnosine. XRD patterns confirmed that both bare and carnosine-modified CeO_2 sols consist of single-phase fluorite-structured cerium dioxide (PDF2 34-0394). Full-pattern analysis of XRD results indicated that the coherent scattering region dimensions of the CeO_2 powders ranged from 2.7 to 3.4 nm (Table 1). Thus, modification of the CeO_2 sol with carnosine did not affect the phase composition of the solid phase, as evidenced by the unchanged positions of the (111), (200), (220), and (311) reflections (see Supplementary Information, Figure S1a).

Table 1. Particle size and ζ-potential of bare and carnosine-coated CeO_2 nanoparticles

Sample	Particle size, nm	ζ, mV
Bare CeO_2	2.7 ± 0.2	32.6 ± 0.5
Carnosine-coated CeO_2	3.4 ± 0.1	5.4 ± 0.2

Figure S1b (see Supplementary Information, Figure S1b (after references section)) presents the size distribution of cerium dioxide particles in aqueous solutions measured by dynamic light scattering (DLS). The bare CeO_2 sol contained aggregates with sizes ranging from 10 to 30 nm. Functionalization of the cerium dioxide sol with carnosine resulted in larger aggregates, with size modes of approximately 65 nm and 335 nm.

For bare CeO_2 nanoparticles, the ζ-potential was +32.6 ± 0.5 mV (Table 1), indicating high electrostatic stability of the colloidal system. Coating CeO_2 nanoparticles with carnosine reduced

the ζ-potential to approximately +5.4 mV (Table 1). Partial neutralization of the nanoparticle surface charge decreases electrostatic repulsion, allowing particles to approach one another more closely and promoting the formation of larger aggregates (see Supplementary Information, Figure S1b). This is further supported by the broader dispersion observed in the hydrodynamic diameter distribution.

To confirm the reproducibility of the synthesis and long-term stability of sol, we established that gradually adding a diluted CeO_2 sol to an equal volume of ligand solution is essential for obtaining a stable carnosine-coated cerium dioxide sol. This protocol proved highly reproducible across multiple batches (n = 3). The sol retained its aggregate stability without visible precipitation for at least two months, as supported by zeta potential monitoring. The measured values were +23.7 ± 0.3 mV (day 1), +5.4 ± 0.2 mV (month 2), and +1.01 ± 0.03 mV (month 3). Despite this gradual decrease, which we attribute to the slow oxidation of the ligand molecules, the colloidal stability was maintained for this period.

Spectral characterization

Figure S1c (see Supplementary Information, Figure S1c) presents the UV–Vis absorption spectra of CeO_2 solutions and pure carnosine. Both bare and carnosine-coated CeO_2 sols display an absorption band in the 280–300 nm range, characteristic of nanoscale cerium dioxide, which is consistent with previous reports (35). Hence, coating CeO_2 nanoparticles with carnosine did not change the sol's optical absorption properties.

The infrared spectrum of pristine cerium oxide (see Supplementary Information, Figure S1d) includes a broad absorption band at 3550–3200 cm^{-1}, corresponding to antisymmetric and symmetric O–H stretching vibrations (36, 37). The band in the 1630–1600 cm^{-1} range is assigned to H–O–H bending vibrations. Low-intensity bands at 1440 cm^{-1} and 1280 cm^{-1} correspond to with residual nitrate ions adsorbed on the CeO_2 surface (36, 37). The Ce–O bond stretching vibrations appear in the 480–430 cm^{-1} region.

The FTIR spectrum of carnosine (see Supplementary Information, Figure S1d) shows a band at 3240 cm^{-1} characteristic of $–NH_2$ stretching vibrations (38, 39), overlapping with a broad O–H stretching band. Asymmetric and symmetric stretching of carboxylate anions are observed at 1563 cm^{-1} and 1406 cm^{-1}, respectively. A peak at 2855 cm^{-1} is attributed to symmetric C–H stretching (38), and the band at 1643 cm^{-1} is characteristic of absorbed water (38) (40). In the FTIR spectrum of carnosine-coated nanoceria (see Supplementary Information, Figure S1d), a new absorption band appears at 477 cm^{-1}, corresponding to Ce–O stretching vibrations, confirming the presence of CeO_2 in the composite. The composite spectrum also shows shifts in the carnosine carboxylate bands from 1563 to 1553 cm^{-1} and from 1406 to 1384 cm^{-1}, indicating interaction between the ligand and the CeO_2 nanoparticle surface. Similar spectral shifts have been reported for carnosine-coated iron oxide nanoparticles (38).

Cell viability and mitochondrial potential

A standardized 72-h MTT assay (3-(4,5-dimethylthiazol-2-yl)-2,5-diphenyltetrazolium bromide) was used to evaluate cytotoxicity (Figure 1a), and the TMRM assay (tetramethylrhodamine methyl ester) was employed to assess mitochondrial membrane potential (Figure 1b). Carnosine-coated nanoceria exhibited cytotoxicity at concentrations above 0.53 mM.

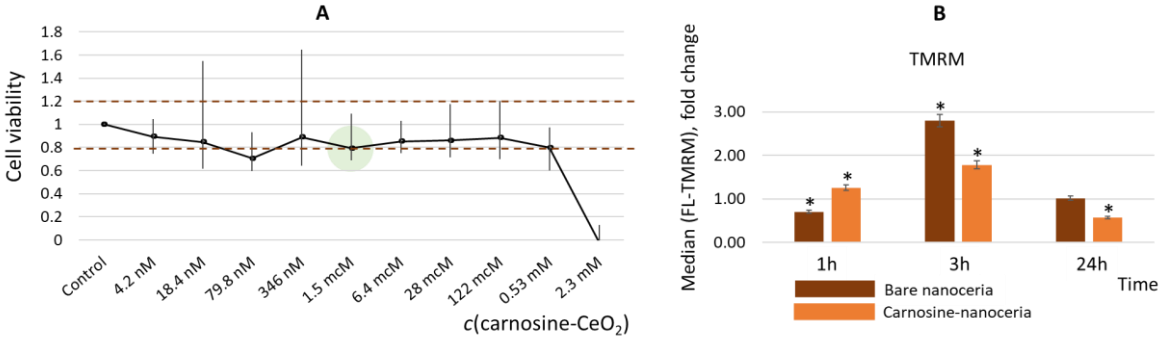

Fig. 1. (A) Cell viability of carnosine-coated nanoceria assessed using the 72-h MTT assay, where the brown dotted lines indicate the viability limits of 80%–120%; the green circle marks the 1.5 µmol/L concentration selected for further experiments; (**B**) mitochondrial membrane potential in cells exposed to bare and carnosine-coated nanoceria (1.5 µmol/L) compared with control values. Here, asterisks denote statistically significant differences in the Mann–Whitney U test with Bonferroni correction (p = 0.004). Both in panels A and B, control cells were incubated without nanoparticles.

In selecting concentrations for studying gene and protein expression, we primarily relied on a proven safe concentration and existing literature data. In *in vitro* models, concentrations around 1 µmol/L are typically used, which ensure system homogeneity, absence of nanoparticle agglomeration, and cell safety (41) (42). In numerous preliminary experiments, we studied nanoceria concentrations ranging from 0.1 to 10 µmol/L and demonstrated a linear effect within this range. Thus, for subsequent experiments, a non-toxic concentration of 1.5 µmol/L—within the middle of the tested range—was selected (highlighted with a green circle in Figure 1a).

Regarding mitochondrial membrane potential, bare and carnosine-coated nanoceria produced similar effects at 3 h and 24 h; however, carnosine functionalization attenuated the impact. Bare nanoceria changed the fluorescence probe intensity by 0.70 times (p = 0.0006) and 2.81 times (p < 0.0001) after 1 and 3 hours of exposure, respectively. Carnosine-coated cerium increased the fluorescence probe intensity by 1.26 times (p = 0.002) after 1 hour of exposure, by 1.78 times (p = 0.001) after 3 hours of exposure, and by 0.57 times (p = 0.0009) after 24 hours of exposure.

Visualization and assessment of intracellular ROS quantity

Since nanoceria exhibits intrinsic red fluorescence (43), we obtained fluorescence micrographs of cells incubated with 1.5 µmol/L nanoparticles for 3 h. The images indicate that carnosine-coated CeO_2 nanoparticles successfully enter the cells (Figure 2)

The internalization was studied by measuring the fluorescence of cells in the red channel of a flow cytometer (Figure 3). The data indicate that the nanoparticles are efficiently internalized into the cells.

Quantification of intracellular reactive oxygen species was performed by flow cytometry employing 2′,7′-dichlorodihydrofluorescein diacetate (H_2DCFH-DA). Pristine CeO_2 exhibited an antioxidant impact after 1 h and 3 h of incubation (fluorescence intensity decreased to 71.8% (p = 0.0012) and 75.5% (p = 0.0011) of control, respectively), whereas carnosine-coated nanoceria induced a 28.0% increase in ROS levels after 24 h (p = 0.0007). (Figure 4)

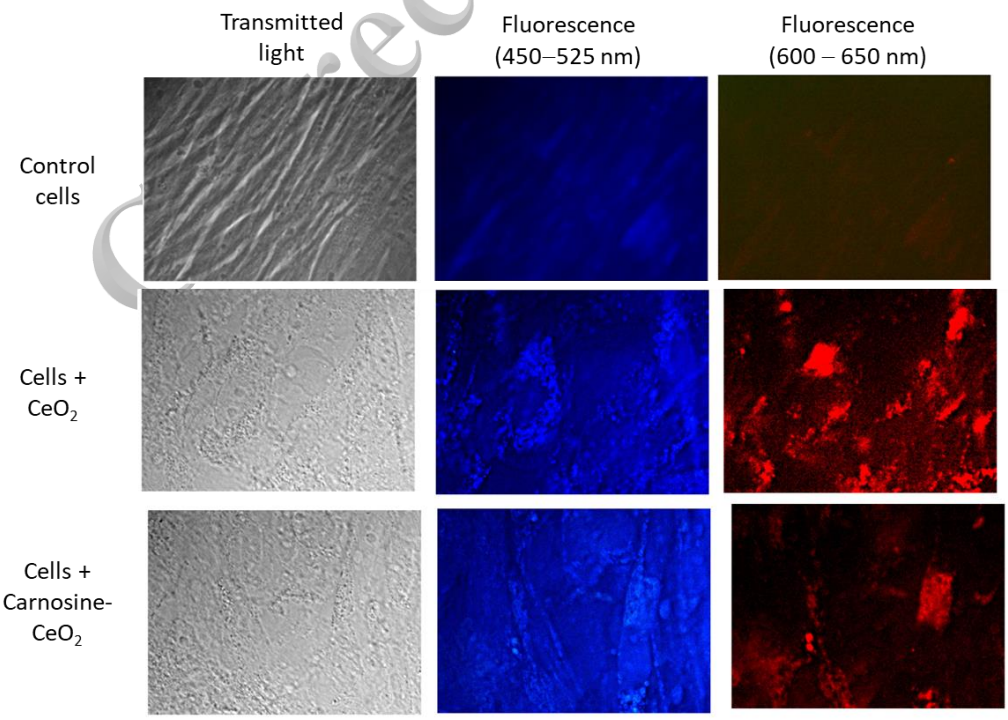

Fig. 2. Visualization of cells during nanoparticle internalization — transmitted-light images (left column) and fluorescence images obtained using a blue filter (middle column, passband 450–525 nm) and a red filter (right column, passband 600–650 nm). The top row shows images of human fetal lung fibroblasts incubated without nanoparticles (control cells); the middle row shows cells after 3 h of exposure to bare nanoceria (1.5 µmol/L); the bottom row shows cells after 3 h of exposure to carnosine-coated nanoceria (1.5 µmol/L); magnification, 100×.

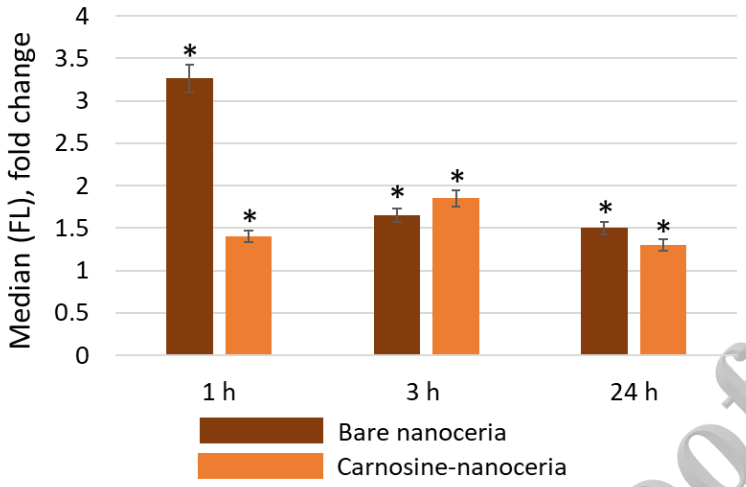

Fig. 3. Fluorescence of cells relative to the control (cells incubated without nanoparticles) after 1, 3, and 24 h of exposure to bare nanoceria and carnosine-coated nanoceria (1.5 µmol/L); asterisks denote statistically significant differences in the Mann–Whitney U test with Bonferroni correction (p = 0.004).

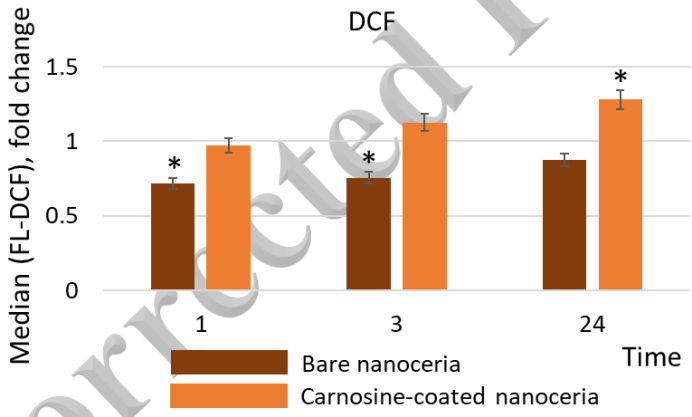

Fig. 4. Intracellular ROS levels relative to control, measured by flow cytometry with dichlorofluorescein (DCF). Cells were exposed to bare or carnosine-coated nanoceria (1.5 µmol/L) for 1, 3, or 24 h; asterisks denote statistically significant differences in the Mann–Whitney U test with Bonferroni correction (p = 0.004). Control cells were incubated without nanoparticles.

Genotoxicity

To assess genotoxicity, quantification of 8-oxo-2'-deoxyguanosine (8-oxo-dG), a biomarker for oxidative DNA damage, and phosphorylated γH2AX, a marker for DNA double-strand breaks, was performed (Figure 5a,b). The DNA repair system function was analyzed through BRCA1 (breast cancer type 1 susceptibility protein) expression measurement (Figure 5c).

For oxidative DNA damage, differences were observed after 1 h of exposure: bare nanoceria reduced oxidative damage to 53.7% of control (p = 0.001) (interquartile range [51.2%; 56.0%]), whereas carnosine-coated nanoceria increased it 1.29-fold (p = 0.002) (Figure 5a). In contrast, for DNA double-strand breaks and BRCA1 protein expression, the response dynamics were similar, with carnosine functionalization exerting a mitigating effect (Figure 5b,c). After 24 hours, γH2AX expression increased 1.38-fold (p = 0.002) in cells incubated with bare nanoceria and 1.34-fold (p = 0.002) in cells incubated with carnosine-coated nanoceria. After 72 hours, γH2AX expression decreased to 23.9% of the control level for bare nanoceria (p < 0.0001) and to 78.7% for carnosine-coated nanoceria (p = 0.0038). The expression of the DNA repair marker — BRCA1 protein decreased to 56.5% after 1 hour of exposure (p = 0.001) and to 68.3% after 72 hours (p = 0.003) for bare nanoceria. For carnosine-coated nanoceria, BRCA1 expression did not differ significantly from the control.

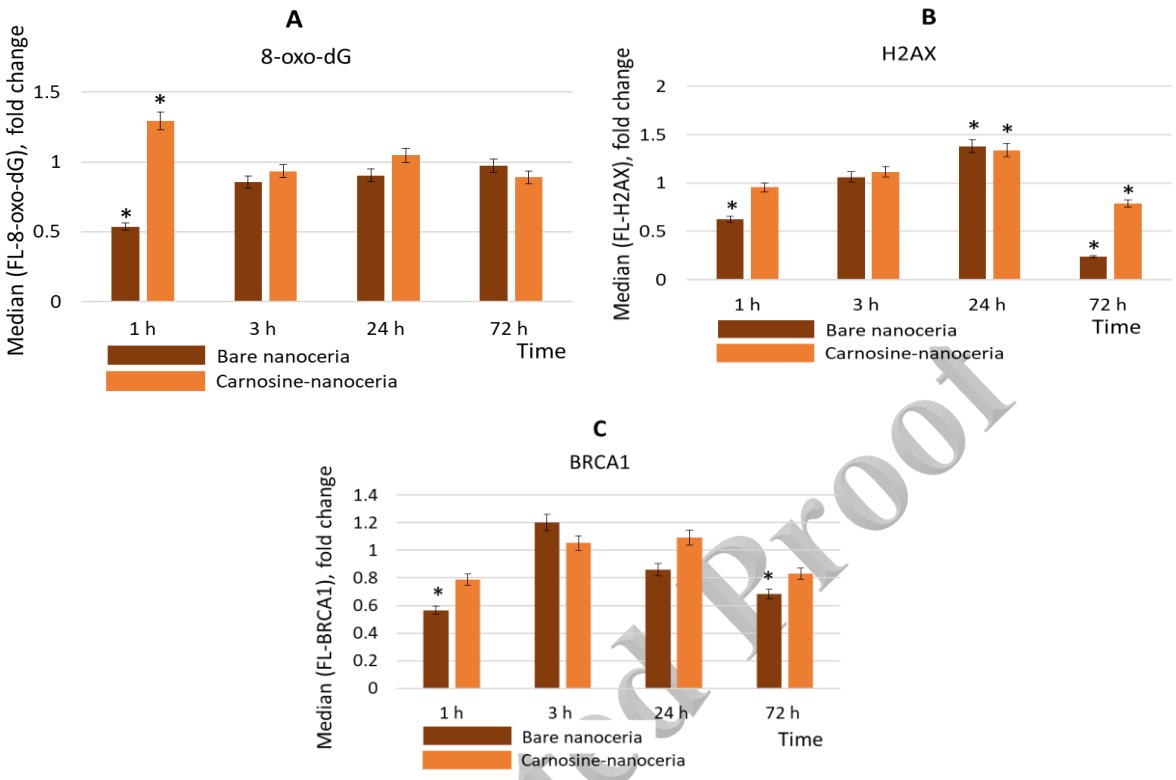

Fig. 5. (A) Concentrations of 8-oxo-2′-deoxyguanosine (8-oxo-dG) relative to control, (B) expression of phosphorylated γH2AX protein relative to control, and (C) expression of BRCA1 protein relative to control values. In all cases, the cells were exposed to bare or carnosine-coated nanoceria (1.5 μmol/L) for 1–72 h; asterisks denote statistically significant differences in the Mann–Whitney U test with Bonferroni correction ($p = 0.004$); control cells were incubated without nanoparticles.

ROS-mediated and inflammatory signaling pathways

NOX4 (NADPH oxidase 4) is a major oxidant enzyme, whereas NRF2 (nuclear factor erythroid 2-related factor 2) is a key regulator of anti-inflammatory and antioxidant responses. For pristine nanoceria, NOX4 expression showed a slight increase after 3 hours of exposure (1.23-fold, $p = 0.004$) and decreased to 64% of control levels after 72 hours ($p = 0.002$) (Figure 6a). For carnosine-coated nanoceria, NOX4 expression decreased to 76.8% of control levels after 72 hours ($p = 0.003$). Changes in NRF2 expression did not reach statistical significance at 1, 3, or 24 h (Figure 6b). Overall, the impacts of pristine and carnosine-conjugated nanoceria were qualitatively similar, although carnosine functionalization again resulted in a less pronounced cellular response.

For STAT3 (signal transducer and activator of transcription 3), bare nanoceria elicited the activating response after 1 h of incubation (1.27-fold increase in expression, $p = 0.002$), followed by a decline to 26.9% of control levels by 72 hours ($p < 0.0001$). In contrast, carnosine-coated nanoceria induced STAT3 activation predominantly after 24 hours of exposure, when expression increased 1.30-fold ($p = 0.001$) (Figure 6c).

Proliferation and autophagy

LC3 (microtubule-associated protein 1 light chain 3) and BECLIN-1 are established autophagy biomarkers. Exposure to either bare or carnosine-coated nanoceria did not result in significant changes in their expression, except for a slight decrease in BECLIN-1 levels at 3 h (to 67.4% for bare nanoceria, $p = 0.003$, to 70.0% for carnosine-coated nanoceria, $p = 0.003$) and 72 h (to 70.0% for bare nanoceria, $p = 0.003$) (Figure 7a,b).

For the proliferation marker PCNA (proliferating cell nuclear antigen), bare nanoceria induced an increase in PCNA expression after 1 hour of incubation by 1.26-fold ($p = 0.003$), however, expression subsequently decreased to 63.9% ($p = 0.0001$) and 23.9% ($p < 0.0001$) of control levels at 24 and 72 hours, respectively. Carnosine-coated nanoceria caused a decrease in PCNA expression after 3 h of exposure to 74.0% of control levels ($p = 0.003$) and after 72 h of exposure to 42.1% of control levels ($p < 0.0001$). A sharp increase in PCNA expression was observed after 24 hours of exposure, reaching 2.36-fold ($p < 0.0000$) (Figure 7c).

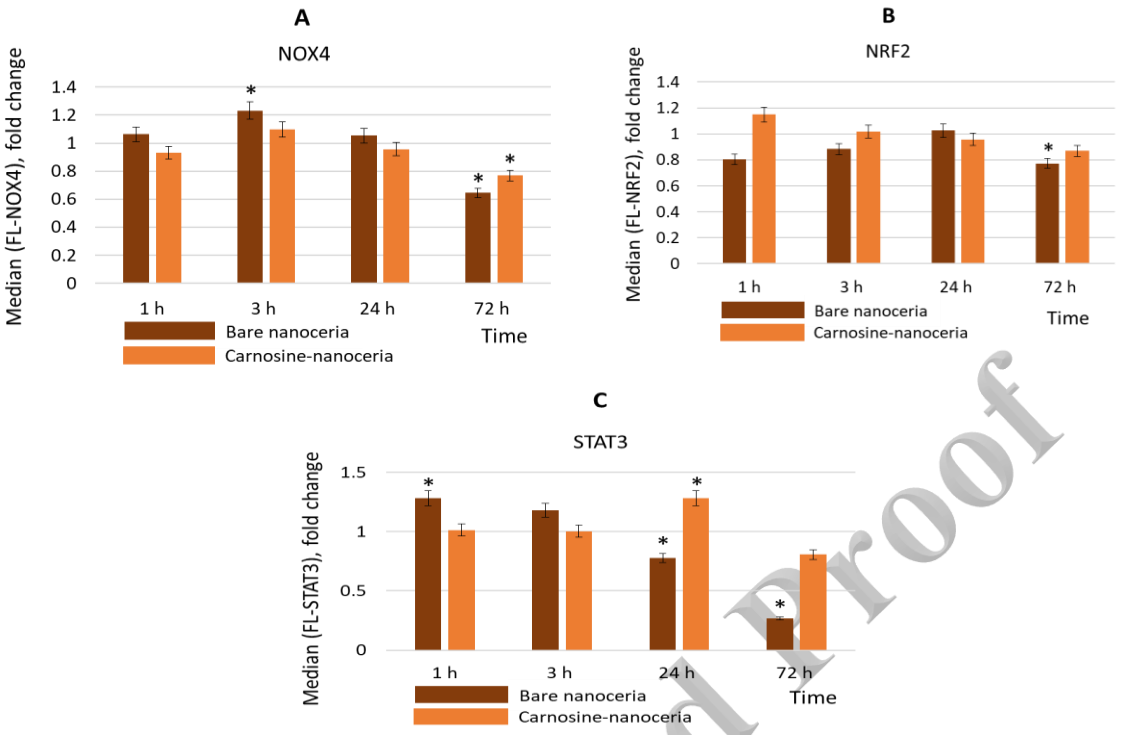

Fig. 6. (A) Expression of NOX4 protein relative to control, (B) expression of NRF2 protein relative to control, and (C) expression of STAT3 protein relative to control. In all cases, the cells were exposed to bare or carnosine coated nanoceria (1.5 µmol/L) for 1–72 h; asterisks denote statistically significant differences in the Mann–Whitney U test with Bonferroni correction (p = 0.004); control cells were incubated without nanoparticles.

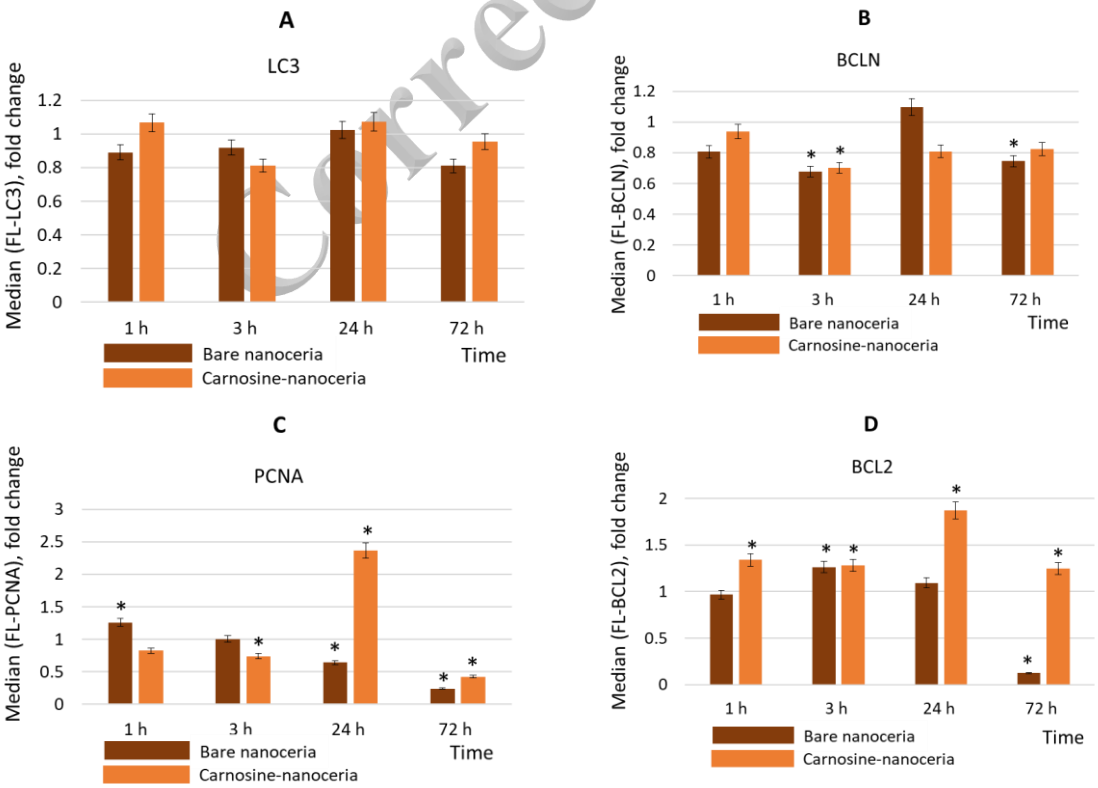

Fig. 7. (A) Expression of LC3 protein relative to control, (B) expression of BECLIN-1 protein relative to control, (C) expression of PCNA protein relative to control, and (D) expression of BCL-2 protein relative to control. In all cases, cells were exposed to bare or carnosine-coated nanoceria (1.5 µmol/L) for 1–72 h; asterisks denote statistically significant differences in the Mann–Whitney U test with Bonferroni correction (p = 0.004); control cells were incubated without nanoparticles.

An anti-apoptotic protein BCL-2 (B-cell lymphoma 2) was differentially affected. Bare nanoceria caused an increase in the expression of this protein by 1.26-fold after 3 hours of exposure (p = 0.003), followed by a sharp decrease to 12.6% of control levels after 72 hours (p < 0.0000). In contrast to bare nanoceria, carnosine-coated nanoceria significantly upregulated BCL-2 expression at at all exposure times (Figure 7d). The expression increase was 1.33-fold (p = 0.002), 1.28-fold (p = 0.003), 1.87-fold (p = 0.0001), and 1.25-fold (p = 0.003) after 1, 3, 27, and 72 hours of exposure, respectively.

Gene expression

We subsequently assessed the expression of selected genes to evaluate whether the observed changes occurred in protein levels were regulated at the transcriptional level. The primary targets included *STAT3*, *BAX*, *BCL2*, *Ki-67* (encoding the proliferation marker protein), *BRCA1*, as well as *NOX4*, *NF-κB*, and *NRF2*. Based on the pronounced activation of the STAT3/BCL2 axis at 1 h and 24 h, these two exposure times were selected for analysis (Figure 8).

The results confirmed activation of *STAT3*, *BCL2*, and *Ki-67* gene expression at 24 h, with minimal or no effect on the ROS-dependent genes *NOX4*, *NF-κB*, and *NRF2*, and no effect on the pro-apoptotic *BAX* or DNA repair *BRCA1* genes. After 24 h, *STAT3* mRNA expression increased 1.73-fold (p < 0.0001), *BCL2* gene expression increased 1.96-fold (p = 0.002), and *Ki-67* gene expression increased 2.21-fold. (p < 0.0001) These findings support the hypothesis that carnosine-coated nanoceria activates the STAT3/BCL2 axis, most likely through a direct mechanism independent of ROS-mediated pathways.

To sum, carnosine functionalization modifies the cellular response to nanoceria, enhancing survival- and proliferation-associated signaling through the STAT3/BCL2 axis while maintaining low overall cytotoxicity, thus highlighting its potential as a targeted nanobiomaterial for biomedical applications.

DISCUSSION

The experimental data reveal that carnosine-coated nanoceria exhibits many similarities to bare nanoceria in terms of cytotoxicity, genotoxicity, DNA repair, mitochondrial potential, autophagy, as well as NOX4 and NRF2 protein expression. However, notable differences arise in the activation of STAT3, PCNA, and BCL2 proteins, where carnosine-coated nanoceria induces a pronounced activating effect after 24 hours of exposure. Additionally, carnosine-coated nanoceria. creates a more oxidative intracellular environment following 24 hours of exposure. It should be noted that excessive intracellular reactive oxygen species did not lead to oxidative DNA damage, and overall, the studied nanoparticles do not exhibit genotoxicity. The absence of oxidative DNA damage indicates sufficient antioxidant capacity within the cell, possibly enhanced by the antioxidant potential of carnosine.

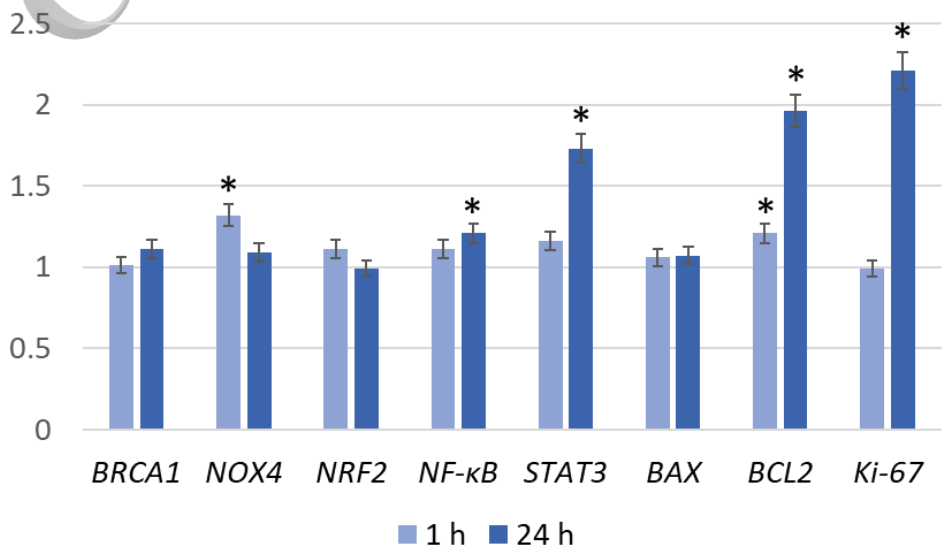

Fig. 8. Relative gene expression in cells exposed to carnosine-coated nanoceria (1.5 μmol/L) for 1 h and 24 h, compared with control values. '*' denotes statistically significant differences in the Mann–Whitney U test with Bonferroni correction (p = 0.005). Control cells were incubated without nanoparticles.

STAT3 is a pivotal component of the JAK/STAT signaling cascade. Upon activation by phosphorylation, STAT3 translocates to the nucleus, where it regulates gene transcription. STAT3 is extensively studied as a prospective target for therapy in cancer due to its frequent overexpression across diverse tumor types, where it promotes cancer cell proliferation, survival, invasion, stemness, angiogenesis, and resistance to chemotherapy (44) (45). The JAK/STAT cascade, especially involving Janus kinases associated with cytokine receptors, plays an important role in mediating inflammatory signaling downstream of IL-6 and IL-10 cytokines in inflammation and cancer (46) (47). Beyond oncology, STAT3 inhibition is being explored as a potential treatment strategy for neurodegenerative diseases (48), cardiac fibrosis (49), and bone diseases (50), although effective clinical antagonists remain under development (51).

The JAK/STAT3 signaling pathway interacts closely with other major signaling cascades such as PI3K/AKT/mTOR and MAPK/ERK (52), and its activity is finely modulated by oxidative stress (53). Specifically, hydrogen peroxide can inhibit intracellular tyrosine phosphatases, which leads to enhanced STAT3 tyrosine phosphorylation (54). Interestingly, oxidative stress not only activates STAT3 but also maintains cytokine-induced STAT3 phosphorylation and its active state in the nucleus (55). Antioxidants like alantolactone and resveratrol have been shown to effectively reduce STAT3 activation by counteracting oxidative stress (56), (57). In our study, while intracellular hydrogen peroxide levels were elevated after exposure to carnosine-coated nanoceria, the lack of significant changes in NOX4 and NRF2 expression casts some doubt on oxidative stress being the sole cause of STAT3 activation. his suggests that the STAT3 activation observed may stem from a direct effect of the carnosine coating itself, possibly through mechanisms independent of classical ROS signaling. Nevertheless, the increased oxidative environment may still contribute to sustaining or supporting STAT3 activation alongside this direct activation. This nuanced interplay points to a complex regulatory network where carnosine-coated nanoceria modulates STAT3 activity both directly and indirectly, highlighting its potential for targeted modulation of cellular survival and proliferation pathways.

The close association between STAT3, BCL2, and PCNA expression in our study is well supported by extensive literature demonstrating their interconnected roles in regulating cell survival, proliferation, and apoptosis inhibition. Alas *et al*. showed that Bcl-2 expression is controlled by the STAT3 signaling pathway, which is modulated by endogenously secreted IL-10 (58). Primary B-cell lymphoma tissues demonstrated a strong linkage between STAT3 expression or phosphorylation and Bcl-2 levels (59). Phospholipase D regulates Bcl-2 expression through activation of the STAT3 signaling pathway (60). STAT3 inactivation reduced PCNA, CyclinD1, and Bcl2 expression in glioma cells (61). STAT3 inhibitor ethanol extract of *Spica Prunellae* resulted in an increase in the proapoptotic Bax/Bcl-2 ratio and a decrease in the expression of proproliferative Cyclin D1 and CDK4 ultimately leading to the activation of apoptosis and inhibition of cell proliferation in colorectal cancer (62). Activation of STAT3 in a mouse model of photocarcinogenesis led to increased transcription of the proliferative and antiapoptotic genes PCNA, Cyclin-D1, Bcl-2, and Bcl-xl (63). STAT 3 activation following polyamine depletion enhances transcription and expression of Bcl-2 and IAP anti-apoptotic proteins and consequently enhancing resistance to tumor necrosis factor-alpha-induced apoptosis (64). Phosphatidic acid increases Bcl-2 expression via STAT3 activation (65). The JAK2/STAT3 signaling cascade plays a critical role in the proliferation of damaged vessel wall cells, which is accompanied by an increase in PCNA (66). Thus, the close association of STAT3 and BCL2 allows their integration into the IL-10/STAT3/BCL2 axis (67) and TYK2/STAT3/Bcl2 (68), which are the basis of chemoresistance and inhibition of apoptosis. The synergistic change in the expression of STAT3, BCL2 and PCNA in our studies indicates that carnosine-coated nanoceria does indeed affect this signaling pathway.

There is some data on the anti-proliferative effect of carnosine in cancer, although the full mechanism is unclear. Rybakova *et al*. showed that carnosine selectively inhibited the proliferation of human glioblastoma cells compared to breast and oral cavity cancer cells (69). In cultured rat pheochromocytoma cells, carnosine led to a slowdown in cell proliferation (70). Carnosine inhibited the proliferation of human colon cancer HCT116 cells (71). Carnosine suppressed the proliferation of human colorectal cancer cells through reduction of beta-catenin/Tcf-4 signaling, induction of both autophagy and necroptosis, and inhibition of angiogenesis-related processes (72). Carnosine demonstrates significant suppression on the proliferation of human cervical carcinoma cells *via* effects on mitochondrial bioenergetics and glycolytic pathways and the cell cycle (73).

On the other hand, L-carnosine contributes significantly to apoptosis inhibition by activating

the anti-apoptotic protein BCL2. Neuronal apoptosis induced by acute cerebral ischemia was suppressed by carnosine through activation of the STAT3/Bcl2 signaling cascade (74). Carnosine was effective in protecting rat liver from ethanol damage by maintaining glutathione levels and BCL2 expression (75), and in protecting the retina from ischemic damage also by increasing BCL2 expression (76). The neuroprotective effect of carnosine in a mouse model of aging is based on a decrease in malondialdehyde and ROS levels and an increase in BCL2 expression (77). Carnosine treatment significantly increased BCL2 levels in lipopolysaccharide-treated *Caenorhabditis elegans*, protecting them from apoptosis (78). Carnosine inhibited apoptosis in H_2O_2-damaged human kidney tubular epithelial cells (79). In a rat acute kidney injury model, carnosine decreased Bax expression and increased Bcl2 expression, inhibiting renal tissue damage and improving survival (80). In frozen and thawed cattle embryos, addition of carnosine to the preservation solution significantly reduced reactive oxygen species production, decreased apoptosis, and increased *Bcl2* mRNA expression (81). Thus, the increase in BCL2 and PCNA expression in our experiments is consistent with literature data indicating the anti-apoptotic and proliferative effect of carnosine.

Thus, we suppose that the activation of STAT3, BCL2 and PCNA is a single pathway and occurs precisely due to carnosine. According to our findings, carnosine-coated nanoceria is found to be an activator of the STAT3/BCL2 axis, which should be taken into account when developing applications. Although the activation of the STAT3/BCL2 axis often needs to be suppressed, since this pathway is associated with increased cancer cell survival, anti-apoptosis, angiogenesis, and chemoresistance (82) (83), in some cases the active STAT3/BCL2 pathway is necessary to inhibit apoptosis. Oritani *et al.* showed that STAT3/BCL2 activation inhibits IL-6-induced apoptosis of macrophages (84). Sepulveda *et al.* proved that IL-6-mediated STAT3 activation supports an anti-apoptotic beneficial effect in human cord blood CD34+ cells, primarily due to bcl-2 overexpression, which is useful for optimizing *ex vivo* cultures for clinical applications (85). Lee *et al.* demonstrated that Deficiency in Stat3 may predispose T cells to apoptosis by attenuating Bcl-2 and Bcl-xL (86). We propose that carnosine-coated nanoceria, as an activator of the STAT3/BCL2 pathway with negligible impact on the oxidative intracellular balance, may be considered a potential agent for promoting the survival of ex vivo cell cultures or organs. Thus, several biomedical scenarios can be proposed for the future practical application of the studied hybrid nanomaterial: a) optimizing *ex vivo* expansion and transplantation of hematopoietic stem cells, b) host defense and intestinal epithelial maintenance, where STAT3 activation regulates antimicrobial peptide expression and suppresses apoptosis, supporting barrier integrity and defense against intestinal infections, c) under conditions of stress or nutrient deficiency, STAT3 pathway activation will promote cell survival, which may be useful in tissue regeneration and wound healing after injuries. However, additional research is necessary to comprehensively understand the biological capabilities of this nanomaterial.

LIMITATIONS

In our study, we proposed the hypothesis of proliferation activation via the STAT3/BCL2 signaling pathway, based on measurements of reporter gene and signaling pathway protein expression under exposure to carnosine-coated nanoceria. However, to confirm this hypothesis, mechanistic experiments using inhibitors or specific siRNA/shRNA knockdown of key signaling components should be conducted.

CONCLUSIONS

Using an *in vitro* model of human embryonic lung fibroblasts, we investigated the impacts of carnosine-coated nanoceria on cell survival, cellular uptake, intracellular ROS balance, genotoxicity and DNA repair systems, markers of proliferation and autophagy, and expression of NOX4, NRF2, and STAT3 proteins and genes. Carnosine-conjugated nanoceria exhibits no cytotoxicity up to 0.53 mM. Within 3 h, both pristine and carnosine-conjugated CeO_2 nanoparticles were efficiently internalized by cells. Carnosine-coated nanoceria behaved similarly to bare nanoceria with respect to cytotoxicity, genotoxicity, DNA repair, effects on mitochondrial membrane potential and autophagy, and regulation of NOX4 and NRF2 proteins. The main differences were observed in the expression of STAT3, PCNA, and BCL2 proteins, where carnosine-coated nanoceria induced a pronounced activating effect after 24 h of exposure. In addition, carnosine-coated nanoceria generated an oxidative intracellular environment after 24 h. We hypothesize that carnosine-coated nanoceria directly activates the STAT3/BCL2 axis while exerting minimal effect on intracellular oxidative metabolism. These findings may aid the development of new molecular models for studying signaling pathways and contribute to biochemical mechanisms of nanoceria as a regulator of cell metabolism. From a practical perspective,

carnosine-coated nanoceria, as an activator of the STAT3/BCL2 pathway with negligible impact on intracellular oxidative balance, may be considered a potential agent for promoting the survival of *ex vivo* cell cultures or organs. However, additional research is necessary to comprehensively understand the biological capabilities of this nanomaterial.

ACKNOWLEDGMENTS

The authors thank Dr. Larisa Kameneva for assistance with cell culturing.

CONFLICTS OF INTEREST

The authors confirm that they have no conflicts of interest to disclose.

FUNDING SOURCES

The research was financially supported by the Russian Science Foundation, project No. 24-13-00370.

ETHICAL CONSIDERATIONS AND CODE

The study was conducted in accordance with the Declaration of Helsinki and approved by the Ethics Committee of the Research Centre for Medical Genetics (Approval #5, 3 July 2017).

AUTHOR CONTRIBUTIONS

The manuscript was written through contributions of all authors. All authors have given approval to the final version of the manuscript.

ARTIFICIAL INTELLIGENCE (AI)

The authors declare that generative artificial intelligence (AI) was not used in the preparation of this article.

REFERENCES

1. Wong LL, McGinnis JF. Nanoceria as bona fide catalytic antioxidants in medicine: what we know and what we want to know. Adv Exp Med Biol. 2014;801:821-828.
2. Saifi MA, Seal S, Godugu C. Nanoceria, the versatile nanoparticles: Promising biomedical applications. J Control Release. 2021;338:164-189.
3. Thakur N, Manna P, Das J. Synthesis and biomedical applications of nanoceria, a redox active nanoparticle. J Nanobiotechnology. 2019;17(1):84.
4. Alvandi M, Shaghaghi Z, Farzipour S, Marzhoseyni Z. Radioprotective Potency of Nanoceria. Curr Radiopharm. 2024;17(2):138-147.
5. Tang JLY, Moonshi SS, Ta HT. Nanoceria: an innovative strategy for cancer treatment. Cell Mol Life Sci. 2023;80(2):46.
6. Kargozar S, Baino F, Hoseini SJ, Hamzehlou S, Darroudi M, Verdi J, Hasanzadeh L, Kim HW, Mozafari M. Biomedical applications of nanoceria: new roles for an old player. Nanomedicine (Lond). 2018;13(23):3051-3069.
7. Sadidi H, Hooshmand S, Ahmadabadi A, Javad Hosseini S, Baino F, Vatanpour M, Kargozar S. Cerium Oxide Nanoparticles (Nanoceria): Hopes in Soft Tissue Engineering. Molecules. 2020;25(19).
8. Tisi A, Passacantando M, Ciancaglini M, Maccarone R. Nanoceria neuroprotective effects in the light-damaged retina: A focus on retinal function and microglia activation. Exp Eye Res. 2019;188:107797.
9. Yokel RA, Hussain S, Garantziotis S, Demokritou P, Castranova V, Cassee FR. The Yin: An adverse health perspective of nanoceria: uptake, distribution, accumulation, and mechanisms of its toxicity. Environ Sci Nano. 2014;1(5):406-428.
10. Budzen S, Rymaszewska J. The biological role of carnosine and its possible applications in medicine. Adv Clin Exp Med. 2013;22(5):739-744.
11. Boldyrev AA, Aldini G, Derave W. Physiology and pathophysiology of carnosine. Physiol Rev. 2013;93(4):1803-1845.
12. Cararo JH, Streck EL, Schuck PF, Ferreira Gda C. Carnosine and Related Peptides: Therapeutic Potential in Age-Related Disorders. Aging Dis. 2015;6(5):369-379.
13. Ghodsi R, Kheirouri S. Carnosine and advanced glycation end products: a systematic review. Amino Acids. 2018;50(9):1177-1186.
14. Sale C, Artioli GG, Gualano B, Saunders B, Hobson RM, Harris RC. Carnosine: from exercise performance to health. Amino Acids. 2013;44(6):1477-1491.
15. Creighton JV, de Souza Goncalves L, Artioli GG, Tan D, Elliott-Sale KJ, Turner MD, Doig CL, Sale C. Physiological Roles of Carnosine in Myocardial Function and Health. Adv Nutr. 2022;13(5):1914-1929.
16. Feehan J, Hariharan R, Buckenham T, Handley C, Bhatnagar A, Baba SP, de Courten B. Carnosine as a potential therapeutic for the management of peripheral vascular disease. Nutr Metab Cardiovasc Dis. 2022;32(10):2289-2296.
17. Yang H, Hou X, Xing L, Tian F. Carnosine and bone (Review). Mol Med Rep. 2023;27(1).
18. Berezhnoy DS, Stvolinsky SL, Lopachev AV, Devyatov AA, Lopacheva OM, Kulikova OI, Abaimov DA, Fedorova TN. Carnosine as an effective neuroprotector in brain pathology and potential neuromodulator in normal conditions. Amino Acids. 2019;51(1):139-150.
19. Babizhayev MA. The detox strategy in smoking comprising nutraceutical formulas of non-hydrolyzed carnosine or carcinine used to protect human health. Hum Exp Toxicol. 2014;33(3):284-316.
20. Caruso G, Privitera A, Antunes BM, Lazzarino G, Lunte SM, Aldini G, Caraci F. The Therapeutic Potential of Carnosine as an Antidote against Drug-Induced Cardiotoxicity and Neurotoxicity: Focus on Nrf2 Pathway. Molecules. 2022;27(14).
21. Zhou JY, Lin HL, Qin YC, Li XG, Gao CQ, Yan HC, Wang XQ. l-Carnosine Protects Against Deoxynivalenol-Induced Oxidative Stress in Intestinal Stem Cells by

Regulating the Keap1/Nrf2 Signaling Pathway. Mol Nutr Food Res. 2021;65(17):e2100406.
22. Prokopieva VD, Yarygina EG, Bokhan NA, Ivanova SA. Use of Carnosine for Oxidative Stress Reduction in Different Pathologies. Oxid Med Cell Longev. 2016;2016:2939087.
23. Artioli GG, Sale C, Jones RL. Carnosine in health and disease. Eur J Sport Sci. 2019;19(1):30-39.
24. Hipkiss AR, Baye E, de Courten B. Carnosine and the processes of ageing. Maturitas. 2016;93:28-33.
25. McFarland GA, Holliday R. Retardation of the senescence of cultured human diploid fibroblasts by carnosine. Exp Cell Res. 1994;212(2):167-175.
26. McFarland GA, Holliday R. Further evidence for the rejuvenating effects of the dipeptide L-carnosine on cultured human diploid fibroblasts. Exp Gerontol. 1999;34(1):35-45.
27. Shao L, Li QH, Tan Z. L-carnosine reduces telomere damage and shortening rate in cultured normal fibroblasts. Biochem Biophys Res Commun. 2004;324(2):931-936.
28. Ketabi S, Rahmani L. Carbon nanotube as a carrier in drug delivery system for carnosine dipeptide: A computer simulation study. Mater Sci Eng C Mater Biol Appl. 2017;73:173-181.
29. Gholibegloo E, Karbasi A, Pourhajibagher M, Chiniforush N, Ramazani A, Akbari T, Bahador A, Khoobi M. Carnosine-graphene oxide conjugates decorated with hydroxyapatite as promising nanocarrier for ICG loading with enhanced antibacterial effects in photodynamic therapy against Streptococcus mutans. J Photochem Photobiol B. 2018;181:14-22.
30. Farid RM, Gaafar PME, Hazzah HA, Helmy MW, Abdallah OY. Chemotherapeutic potential of L-carnosine from stimuli-responsive magnetic nanoparticles against breast cancer model. Nanomedicine (Lond). 2020;15(9):891-911.
31. Lu X, Zhang Y, Wang L, Li G, Gao J, Wang Y. Development of L-carnosine functionalized iron oxide nanoparticles loaded with dexamethasone for simultaneous therapeutic potential of blood brain barrier crossing and ischemic stroke treatment. Drug Deliv. 2021;28(1):380-389.
32. Homaeigohar S, Kordbacheh D, Banerjee S, Gu J, Zhang Y, Huang Z. Zinc Oxide Nanoparticle Loaded L-Carnosine Biofunctionalized Polyacrylonitrile Nanofibrous Wound Dressing for Post-Surgical Treatment of Melanoma. Polymers (Basel). 2025;17(2).
33. Shcherbakov AB, Teplonogova MA, Ivanova OS, Shekunova TO, Ivonin IV, Baranchikov AY, Ivanov VK. Facile method for fabrication of surfactant-free concentrated CeO2 sols. Materials Research Express. 2017;4(5):055008.
34. Creed S, McKenzie M. Measurement of Mitochondrial Membrane Potential with the Fluorescent Dye Tetramethylrhodamine Methyl Ester (TMRM). Methods Mol Biol. 2019;1928:69-76.
35. Huang Y-C, Wu S-H, Hsiao C-H, Lee A-T, Huang MH. Mild synthesis of size-tunable CeO2 octahedra for band gap variation. Chemistry of Materials. 2020;32(6):2631-2638.
36. Prabaharan DMDM, Sadaiyandi K, Mahendran M, Sagadevan S. Structural, optical, morphological and dielectric properties of cerium oxide nanoparticles. Materials Research. 2016;19(2):478-482.
37. Sozarukova M, Proskurnina E, Mikheev I, Polevoy L, Baranchikov A, Ivanov V. Anti-and Pro-Oxidant Properties of Cerium Oxide Nanoparticles Functionalized with Gallic Acid. Russian Journal of Inorganic Chemistry. 2023;68(8):1108-1116.
38. Durmus Z, Kavas H, Baykal A, Sozeri H, Alpsoy L, Çelik S, Toprak M. Synthesis and characterization of l-carnosine coated iron oxide nanoparticles. Journal of Alloys and Compounds. 2011;509(5):2555-2561.
39. Torreggiani A, Tamba M, Fini G. Binding of copper (II) to carnosine: Raman and IR spectroscopic study. Biopolymers: Original Research on Biomolecules. 2000;57(3):149-159.
40. Wagner CC, Baran EJ. Vibrational spectra of polaprezinc, a polymeric Zn (II) complex of carnosine. Journal of Raman Spectroscopy: An International Journal for Original Work in all Aspects of Raman Spectroscopy, Including Higher Order Processes, and also Brillouin and Rayleigh Scattering. 2008;39(4):474-477.
41. Singh S, Ly A, Das S, Sakthivel TS, Barkam S, Seal S. Cerium oxide nanoparticles at the nano-bio interface: size-dependent cellular uptake. Artificial Cells, Nanomedicine, and Biotechnology. 2018;46(sup3):956-963.
42. Bailey ZS, Nilson E, Bates JA, Oyalowo A, Hockey KS, Sajja V, Thorpe C, Rogers H, Dunn B, Frey AS, Billings MJ, Sholar CA, Hermundstad A, Kumar C, VandeVord PJ, Rzigalinski BA. Cerium Oxide Nanoparticles Improve Outcome after In Vitro and In Vivo Mild Traumatic Brain Injury. J Neurotrauma. 2020;37(12):1452-1462.
43. Proskurnina EV, Sozarukova MM, Ershova ES, Savinova EA, Kameneva LV, Veiko NN, Teplonogova MA, Saprykin VP, Ivanov VK, Kostyuk SV. Lipid Coating Modulates Effects of Nanoceria on Oxidative Metabolism in Human Embryonic Lung Fibroblasts: A Case of Cardiolipin. Biomolecules. 2025;15:53.
44. Shi D, Tao J, Man S, Zhang N, Ma L, Guo L, Huang L, Gao W. Structure, function, signaling pathways and clinical therapeutics: The translational potential of STAT3 as a target for cancer therapy. Biochim Biophys Acta Rev Cancer. 2024;1879(6):189207.
45. Hashemi M, Abbaszadeh S, Rashidi M, Amini N, Talebi Anaraki K, Motahhary M, Khalilipouya E, Harif Nashtifani A, Shafiei S, Ramezani Farani M, Nabavi N, Salimimoghadam S, Aref AR, Raesi R, Taheriazam A, Entezari M, Zha W. STAT3 as a newly emerging target in colorectal cancer therapy: Tumorigenesis, therapy response, and pharmacological/nanoplatform strategies. Environ Res. 2023;233:116458.
46. Huynh J, Etemadi N, Hollande F, Ernst M, Buchert M. The JAK/STAT3 axis: A comprehensive drug target for solid malignancies. Semin Cancer Biol. 2017;45:13-22.

47. Kitamura H, Ohno Y, Toyoshima Y, Ohtake J, Homma S, Kawamura H, Takahashi N, Taketomi A. Interleukin-6/STAT3 signaling as a promising target to improve the efficacy of cancer immunotherapy. Cancer Sci. 2017;108(10):1947-1952.
48. Panda SP, Kesharwani A, Datta S, Prasanth D, Panda SK, Guru A. JAK2/STAT3 as a new potential target to manage neurodegenerative diseases: An interactive review. Eur J Pharmacol. 2024;970:176490.
49. Jiang H, Yang J, Li T, Wang X, Fan Z, Ye Q, Du Y. JAK/STAT3 signaling in cardiac fibrosis: a promising therapeutic target. Front Pharmacol. 2024;15:1336102.
50. Li J, Yin Z, Huang B, Xu K, Su J. Stat3 Signaling Pathway: A Future Therapeutic Target for Bone-Related Diseases. Front Pharmacol. 2022;13:897539.
51. Shih PC. Revisiting the development of small molecular inhibitors that directly target the signal transducer and activator of transcription 3 (STAT3) domains. Life Sci. 2020;242:117241.
52. El-Habr EA, Levidou G, Trigka EA, Sakalidou J, Piperi C, Chatziandreou I, Spyropoulou A, Soldatos R, Tomara G, Petraki K, Samaras V, Zisakis A, Varsos V, Vrettakos G, Boviatsis E, Patsouris E, Saetta AA, Korkolopoulou P. Complex interactions between the components of the PI3K/AKT/mTOR pathway, and with components of MAPK, JAK/STAT and Notch-1 pathways, indicate their involvement in meningioma development. Virchows Arch. 2014;465(4):473-485.
53. Xu Z, Wu H, Zhang H, Bai J, Zhang Z. Interleukins 6/8 and cyclooxygenase-2 release and expressions are regulated by oxidative stress-JAK2/STAT3 signaling pathway in human bronchial epithelial cells exposed to particulate matter </=2.5 mum. J Appl Toxicol. 2020;40(9):1210-1218.
54. Carballo M, Conde M, El Bekay R, Martin-Nieto J, Camacho MJ, Monteseirin J, Conde J, Bedoya FJ, Sobrino F. Oxidative stress triggers STAT3 tyrosine phosphorylation and nuclear translocation in human lymphocytes. J Biol Chem. 1999;274(25):17580-17586.
55. Ng IH, Yeap YY, Ong LS, Jans DA, Bogoyevitch MA. Oxidative stress impairs multiple regulatory events to drive persistent cytokine-stimulated STAT3 phosphorylation. Biochim Biophys Acta. 2014;1843(3):483-494.
56. Maryam A, Mehmood T, Zhang H, Li Y, Khan M, Ma T. Alantolactone induces apoptosis, promotes STAT3 glutathionylation and enhances chemosensitivity of A549 lung adenocarcinoma cells to doxorubicin via oxidative stress. Sci Rep. 2017;7(1):6242.
57. Kohandel Z, Farkhondeh T, Aschner M, Pourbagher-Shahri AM, Samarghandian S. STAT3 pathway as a molecular target for resveratrol in breast cancer treatment. Cancer Cell Int. 2021;21(1):468.
58. Alas S, Bonavida B. Rituximab inactivates signal transducer and activation of transcription 3 (STAT3) activity in B-non-Hodgkin's lymphoma through inhibition of the interleukin 10 autocrine/paracrine loop and results in down-regulation of Bcl-2 and sensitization to cytotoxic drugs. Cancer Res. 2001;61(13):5137-5144.
59. Kang J, Chong SJ, Ooi VZ, Vali S, Kumar A, Kapoor S, Abbasi T, Hirpara JL, Loh T, Goh BC, Pervaiz S. Overexpression of Bcl-2 induces STAT-3 activation via an increase in mitochondrial superoxide. Oncotarget. 2015;6(33):34191-34205.
60. Choi HJ, Han JS. Overexpression of phospholipase D enhances Bcl-2 expression by activating STAT3 through independent activation of ERK and p38MAPK in HeLa cells. Biochim Biophys Acta. 2012;1823(6):1082-1091.
61. Tan Y, Huang N, Zhang X, Hu J, Cheng S, Pi L, Cheng Y. KIAA0247 suppresses the proliferation, angiogenesis and promote apoptosis of human glioma through inactivation of the AKT and Stat3 signaling pathway. Oncotarget. 2016;7(52):87100-87113.
62. Lin W, Zheng L, Zhuang Q, Zhao J, Cao Z, Zeng J, Lin S, Xu W, Peng J. Spica prunellae promotes cancer cell apoptosis, inhibits cell proliferation and tumor angiogenesis in a mouse model of colorectal cancer via suppression of stat3 pathway. BMC Complement Altern Med. 2013;13:144.
63. Agilan B, Rajendra Prasad N, Kanimozhi G, Karthikeyan R, Ganesan M, Mohana S, Velmurugan D, Ananthakrishnan D. Caffeic Acid Inhibits Chronic UVB-Induced Cellular Proliferation Through JAK-STAT3 Signaling in Mouse Skin. Photochem Photobiol. 2016;92(3):467-474.
64. Bhattacharya S, Ray RM, Johnson LR. STAT3-mediated transcription of Bcl-2, Mcl-1 and c-IAP2 prevents apoptosis in polyamine-depleted cells. Biochem J. 2005;392(Pt 2):335-344.
65. Choi HJ, Lee JH, Park SY, Cho JH, Han JS. STAT3 is involved in phosphatidic acid-induced Bcl-2 expression in HeLa cells. Exp Mol Med. 2009;41(2):94-101.
66. Zhao J, Zhang M, Li W, Su X, Zhu L, Hang C. Suppression of JAK2/STAT3 signaling reduces end-to-end arterial anastomosis induced cell proliferation in common carotid arteries of rats. PLoS One. 2013;8(3):e58730.
67. Wu D, Wang Z. Gastric Cancer Cell-Derived Kynurenines Hyperactive Regulatory T Cells to Promote Chemoresistance via the IL-10/STAT3/BCL2 Signaling Pathway. DNA Cell Biol. 2022;41(4):447-455.
68. Qin W, Peng C, Yang X, Jiang A, Zhong N, Liu Y, Zhang X, Hirbe AC, Ma M, Yue X. SS18-SSX drives TYK2 expression to activate STAT3/Bcl2 axis, facilitating apoptosis evasion and advancing synovial sarcoma progression. Cell Biol Toxicol. 2024;41(1):8.
69. Rybakova YS, Kalen AL, Eckers JC, Fedorova TN, Goswami PC, Sarsour EH. [Increased manganese superoxide dismutase and cyclin B1 expression in carnosine-induced inhibition of glioblastoma cell proliferation]. Biomed Khim. 2015;61(4):510-518.
70. Rybakova YS, Boldyrev AA. Effect of carnosine and related compounds on proliferation of cultured rat pheochromocytoma PC-12 cells. Bull Exp Biol Med. 2012;154(1):136-140.
71. Iovine B, Iannella ML, Nocella F, Pricolo MR, Bevilacqua MA. Carnosine inhibits KRAS-mediated

HCT116 proliferation by affecting ATP and ROS production. Cancer Lett. 2012;315(2):122-128.
72. Hsieh SL, Li JH, Dong CD, Chen CW, Wu CC. Carnosine suppresses human colorectal cancer cell proliferation by inducing necroptosis and autophagy and reducing angiogenesis. Oncol Lett. 2022;23(2):44.
73. Bao Y, Ding S, Cheng J, Liu Y, Wang B, Xu H, Shen Y, Lyu J. Carnosine Inhibits the Proliferation of Human Cervical Gland Carcinoma Cells Through Inhibiting Both Mitochondrial Bioenergetics and Glycolysis Pathways and Retarding Cell Cycle Progression. Integr Cancer Ther. 2018;17(1):80-91.
74. Wang JP, Yang ZT, Liu C, He YH, Zhao SS. L-carnosine inhibits neuronal cell apoptosis through signal transducer and activator of transcription 3 signaling pathway after acute focal cerebral ischemia. Brain Res. 2013;1507:125-133.
75. Baykara B, Micili SC, Tugyan K, Tekmen I, Bagriyanik H, Sonmez U, Sonmez A, Oktay G, Yener N, Ozbal S. The protective effects of carnosine in alcohol-induced hepatic injury in rats. Toxicol Ind Health. 2014;30(1):25-32.
76. Ji YS, Park JW, Heo H, Park JS, Park SW. The neuroprotective effect of carnosine (beta-alanyl-L-histidine) on retinal ganglion cell following ischemia-reperfusion injury. Curr Eye Res. 2014;39(6):634-641.
77. Dai Z, Lu XY, Zhu WL, Liu XQ, Li BY, Song L, Liu HF, Cai WW, Deng YX, Xu TT, Wang Q, Zhang SJ. Carnosine ameliorates age-related dementia via improving mitochondrial dysfunction in SAMP8 mice. Food Funct. 2020;11(3):2489-2497.
78. Ma J, Xu X, Wang R, Yan H, Yao H, Zhang H, Jiang S, Xu A. Lipopolysaccharide exposure induces oxidative damage in Caenorhabditis elegans: protective effects of carnosine. BMC Pharmacol Toxicol. 2020;21(1):85.
79. Cao Y, Xu J, Cui D, Liu L, Zhang S, Shen B, Wu Y, Zhang Q. Protective effect of carnosine on hydrogen peroxide-induced oxidative stress in human kidney tubular epithelial cells. Biochem Biophys Res Commun. 2021;534:576-582.
80. Wang H, Fang Z, Qiu G, Zhang C, Tang M, Zhou B. Bioprotective and Functional Effect of Carnosine on Sepsis Induced Renal Damage in Male Albino Rat Model through Targeting IL-1beta and TNF-alpha Production. Dokl Biochem Biophys. 2021;500(1):408-414.
81. Ishii T, Mori-Kobayashi K, Nakamura S, Ohkura S, Matsuyama S. Carnosine supplementation in cryopreservation solution improved frozen-thawed bovine embryo viability. J Reprod Dev. 2024;70(5):279-285.
82. Zhuang L, Lee CS, Scolyer RA, McCarthy SW, Zhang XD, Thompson JF, Hersey P. Mcl-1, Bcl-XL and Stat3 expression are associated with progression of melanoma whereas Bcl-2, AP-2 and MITF levels decrease during progression of melanoma. Mod Pathol. 2007;20(4):416-426.
83. Ma J, Song X, Xu X, Mou Y. Cancer-Associated Fibroblasts Promote the Chemo-resistance in Gastric Cancer through Secreting IL-11 Targeting JAK/STAT3/Bcl2 Pathway. Cancer Res Treat. 2019;51(1):194-210.
84. Oritani K, Tomiyama Y, Kincade PW, Aoyama K, Yokota T, Matsumura I, Kanakura Y, Nakajima K, Hirano T, Matsuzawa Y. Both Stat3-activation and Stat3-independent BCL2 downregulation are important for interleukin-6-induced apoptosis of 1A9-M cells. Blood. 1999;93(4):1346-1354.
85. Sepulveda P, Encabo A, Carbonell-Uberos F, Minana MD. BCL-2 expression is mainly regulated by JAK/STAT3 pathway in human CD34+ hematopoietic cells. Cell Death Differ. 2007;14(2):378-380.
86. Lee JK, Won C, Yi EH, Seok SH, Kim MH, Kim SJ, Chung MH, Lee HG, Ikuta K, Ye SK. Signal transducer and activator of transcription 3 (Stat3) contributes to T-cell homeostasis by regulating pro-survival Bcl-2 family genes. Immunology. 2013;140(3):288-300.

SUPPLEMENTARY INFORMATION

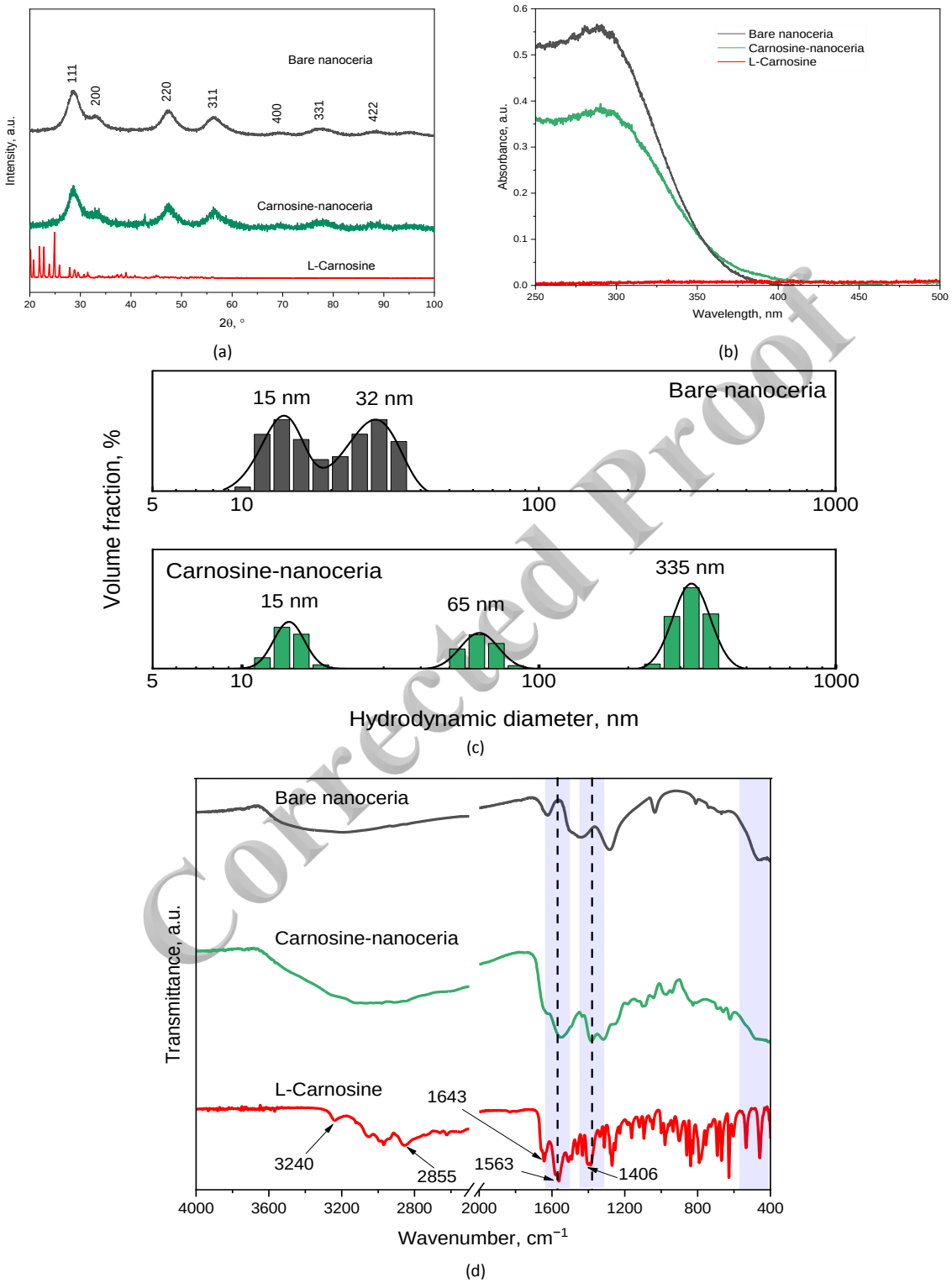

Fig. S1. (a) XRD patterns of the dried ceria sols and pure carnosine; (b) UV-Vis absorption spectra of the ceria sols and pure carnosine; (c) hydrodynamic diameter distributions of the ceria sols; (d) FTIR spectra of the nanoceria sols and pure carnosine.